ROYAL SOCIETY OF CHEMISTRY

COMMUNICATION

Check for updates

Electrolyte tuning with low concentrations of additive for dendrite suppression in lithium metal anodes†

Abiral Baniya,‡[a] Madan Bahadur Saud, [iD]‡[a] Hansheng Li,[a] M. Bilal Faheem, [iD][a] Yuchen Zhang,[a] Ashok Thapa,[b] Raja Sekhar Bobba,[a] Poojan Indrajeet Kaswekar[a] and Quinn Qiao [iD]*[a]

Lithium (Li) metal is considered to be an ideal anode for high-energy density storage systems. However, its high reactivity and instability towards organic electrolytes leads to continuous consumption of electrolytes and Li metal, causing dendrite growth. This induces safety issues and low cyclability, which hinders its practical use. Although electrolyte additives are extensively utilized to address these issues, the practice remains challenging due to the least understanding of their interactions with electrolytic environments. Here, we report a novel electrolyte additive, gadolinium nitrate ($Gd(NO_3)_3$), with a low optimal concentration of 3 mM in a lithium bis(trifluoromethanesulfonyl)imide-lithium nitrate ($LiTFSI$-$LiNO_3$) ether-based electrolyte; this additive promotes plating/stripping of Li in nodular morphology, significantly suppressing dendrites and dead Li growth while improving the cycle life and overall stability of Li metal batteries. A significant reduction is observed in the Li-metal electrode overpotential under a current density of 2 mA cm^{-2}. When a Li metal battery was tested with $LiFePO_4$ (LFP) cathode at an active mass loading of 4 mg cm^{-2}, a capacity retention of 98.33% was observed after 400 cycles. Such stable cycling and enhanced performance are attributed to the formation of a chemically stable, mechanically robust, and ionically conductive solid electrolyte interphase (SEI) layer on the Li metal surface, which is enabled by the incorporation of $Gd(NO_3)_3$ compared to cells with pristine Li electrolytes.

1. Introduction

Rechargeable lithium-metal battery (LMB) is a developing technology with vast potential for numerous applications, such as smart consumer electronics, electric vehicles, and smart grids. Li metal is considered to be an ideal candidate for anodes due to its ultrahigh theoretical specific capacity of

[a]*Energy Conversion and Storage Lab, Mechanical and Aerospace Engineering, Syracuse University, Syracuse, NY 13244, USA. E-mail: quqiao@syr.edu*

[b]*Multiscale Research and Engineering Lab, Mechanical and Aerospace Engineering, Syracuse University, Syracuse, NY 13244, USA*

† Electronic supplementary information (ESI) available. See DOI: https://doi.org/10.1039/d4se00548a

‡ These authors contributed equally.

3860 mA h g^{-1}, low redox potential (-3.040 V *versus* standard hydrogen electrode, SHE), and small gravimetric density of 0.534 g cm^{-3}.[1] All these characteristics indicate the huge potential of rechargeable batteries with Li metal anodes (LMAs) to provide very high capacity and energy density, such as in Li–S batteries[2,3] and potential integration with renewable energy sources, such as solar and wind.[4–6] However, there are still a few cruxes yet to be resolved before their commercialization.

One major challenge is still the growth of Li dendrites and penetration of dead Li through the separator, which can cause abrupt short-circuiting and combustion.[7–10] Non-uniform Li deposition and uncontrolled volumetric change in Li electrodes through plating/stripping will lead to dendritic Li growth and the formation of dead Li on the surface of an LMA. To address this, an SEI passivation layer capable of serving as a strong electrochemical barrier between the electrolyte and LMA is needed to prevent side chain reactions while allowing effortless Li-ion transport. The SEI layer is usually formed from the sacrificial decomposition of electrolytes during the formation cycles.[11] The consumption of Li and the electrolyte decomposition during the initial SEI layer formation increase the impedance to Li-ion transport and the irreversible capacity loss occurs during the charge/discharge cycle.[12,13] A weak and unstable SEI is incapable of suppressing side reactions, but continuous dendrite growth incurs Li inventory loss, continuous electrolyte consumption, continuous capacity fading, and remarkably low coulombic efficiency (CE).[14]

Various innovative approaches have been reported for suppressing dendritic/dead lithium growth on LMAs to improve the cycling stability of lithium metal batteries, including polymer or solid-state electrolytes,[15–17] ionic liquids,[18–20] leakage-responsive electrolyte,[21] concentrated electrolytes and additives,[22,23] artificial protective layers,[24–30] porous current collectors,[31] and Li hosts with nanoscale design and selective deposition.[32–36] Although these approaches have demonstrated remarkable breakthroughs in Li dendrite suppression, their economic feasibility due to complicated synthesis and processing proves to be a major disadvantage.[37–41] Although the SEI layer

formation is essential to suppress the side reactions, the undesired consequences that arise despite its protective nature should be addressed. Employing advanced formulations for liquid electrolytes, such as the inclusion of additives,[42–46] increasing electrolyte salt concentrations,[23,47,48] using dual-salt electrolytes,[49,50] and incorporating novel salt-solvents,[51–54] have been reported to be cost-effective methodologies that are attracting the attention of researchers in developing advanced LMBs with suppressed parasitic reactions and dendrite growth. Similarly, it is widely believed that electrolyte additives provide the missing component in thus-formed interphases enabling the advanced passivation layer tailored by additives for enhanced LMB chemistries.[55,56] Trace amounts of electrolyte additives are implemented to sacrificially decompose before the bulk electrolyte components. This leads to the formation of interphases with enhanced protective measures showing low irreversible capacities, low Li-ion transport impedances and longer cycle life.[57–60]

Nitrate-based electrolyte additives, such as MNO_3 (M = Li, Na, K, La, and Cs),[48,61–65] along with other additives, such as P_2S_5 (ref. 66) and LiI,[67] have shown promise in mitigating the polysulfide shuttle effect in lithium–sulfur (Li–S) batteries by the passivation of Li anode surface via enhanced SEI layer. Similarly, $NaNO_3$ (ref. 43) and $LiNO_3$,[68,69] were recently used as additives in ether-based and carbonate-based electrolytes for the long-term cycling performance of Li-ion and LMBs, respectively.

Electrochemical stability is also a critical parameter for electrolytes. State-of-the-art liquid electrolytes contain some form of lithium salts dissolved in mixed solvents of either carbonate, ester, or ether types. Currently, commercialized carbonate-based electrolytes generally show less-than-desirable electrochemical stabilities with a stable voltage window below 4.3 V (versus Li/Li$^+$). This limits their applications in energy-dense LMBs[51,70,71] that need cathodes to possess higher operational voltage windows. Similarly, ester-based electrolytes face difficulty in forming stable SEI films at the LMA surface, leading to continued electrolyte decomposition and Li inventory loss.[38,41,72–81] In comparison to these electrolytes, ether-based electrolytes show enhanced Li metal modification by forming a stable SEI layer and effective dendrite inhibition.[82–85] However, ether-based electrolytes show lower electrochemical stability up to 3.7 V, when paired with high voltage cathodes.[77,86–91] Therefore, it is imperative to understand the match of electrolytes/electrodes and optimal use of electrolyte additives in high-voltage (>4.3 V) LMBs.

In this work, we demonstrate that the use of a very low concentration (3 mM) of $Gd(NO_3)_3$, a novel electrolyte additive, in a $LiTFSI$-$LiNO_3$ ether-based electrolyte stimulates nodular morphology of Li plating/stripping in LMBs. This morphology of Li plating/stripping enables substantial Li dendrite suppression and inhibits the growth of dead or inactive Li, promoting stable cycling of LMBs. The electrolyte additive tunes the SEI layer composition by forming Gd(III) compounds on the surface of Li metal, providing passivation without excessive electrolyte consumption and degradation. The SEI layer formed in the presence of an electrolyte additive also shows fast Li ion

conduction. In addition, the high electrolyte affinity helps achieve prolonged stability of Li symmetrical cells for 1200 hours at a high current density of 2 mA cm^{-2}. An increase in the electrochemical stability window was also observed. When the $Gd(NO_3)_3$ additive amount was optimized to as low as 3 mM, the LFP/Li full cells exhibited excellent cycling and rate performances.

2. Results and discussion

2.1. Morphology of Li deposition and surface properties

Fig. 1 presents SEM images of the Li metal surface acquired during different plating/stripping cycles. These images reveal the morphological evolution of the deposited Li in the LMAs during symmetrical cell cycling. There are observable dendritic structures (Fig. 1a) within the first plating/stripping cycle of the samples without any additives in the electrolyte. The condition worsened upon consecutive cycling for 10 cycles (Fig. 1b) and 100 cycles (Fig. 1c), as verified by the abundant presence of dendritic and dead Li on the LMA surface. Conversely, the cells assembled with an electrolyte containing $Gd(NO_3)_3$ additive showed no visible growth of dendritic Li and facilitated nodular morphology of Li. This is evident from SEM images of the LMAs cycled in cells with the optimized amount of Gd electrolyte additive at cycle numbers 1 (Fig. 1f), 10 (Fig. 1g), and 100 (Fig. 1h).

The Li deposition in micro-sized nodules minimizes the exposed reaction surface area of Li metal with the electrolyte, thus limiting the parasitic side reactions between the LMA and liquid electrolyte (LE). Furthermore, the presence of flat and uniform nodules promotes the stability of the SEI layer compared to the SEI layer with Li dendrites. The latter is prone to cracks and voids, as presented in the real-time optical images in Fig. 1d and e. The colour of the Li metal surface cycled in electrolyte medium without additive changes from shiny silver to dark and dull after only 100 cycles, whereas the sample with additive electrolyte was found to be shiny silver even after 100 cycles. The change in colour to dark and dull layers describes the formation of insulating layers due to the unstable SEI layer incurring uncontrolled side reactions that eventually lead to the consumption of a high volume of electrolytes. The LMA with additive forms a very stable and uniform SEI layer that inhibits any SEI cracking and side reactions improving the passivation of the Li metal surface while maintaining the shiny physical appearance of the sample surface even after 100 cycles. Contact angles were measured to examine the changes in the wettability of the LMA surface due to the inclusion of $Gd(NO_3)_3$ additive into the electrolyte. As shown in ESI Fig. S1b,† the electrolyte without additive showed a lower electrolyte affinity with the Li metal surface and a higher contact angle of 26.20°, whereas the sample with additive had a higher electrolyte affinity and presented a significantly reduced contact angle of 13.50° (ESI Fig. S1d†). The enhanced electrolyte affinity due to the presence of an additive in the electrolyte helped construct a uniform SEI layer on the LMA with almost no cracks and voids, ensuring effective and stable Li metal passivation.

Fig. 1 Scanning electron microscopy (SEM) images of the LMAs at the (a and f) 1st, (b and g) 10th, and (c and h) 100th cycle without (a–c) and with (f–h) Gd(NO$_3$)$_3$ electrolyte additive. Optical images (d and e) show the macroscopic-scale appearance of the respective LMAs after 100 cycles. All SEM images are collected at a scale bar of 20 μm.

To further study the effects of additives in SEI formation and Li metal surface, elemental and surface analyses were performed using energy-dispersive X-ray spectroscopy (EDS). As shown in ESI Fig. S1a,† the EDS spectrum of the LMA cycled in the electrolyte without additive shows the absence of Gd. In contrast, those cycled in electrolyte with additive showed peaks for Gd (ESI Fig. S1c†) along with other elements, such as nitrogen (N), oxygen (O), fluorine (F), and sulfur (S). The presence of Gd on the LMA surface is attributed to the involvement of Gd(NO$_3$)$_3$ in forming the SEI layer on the top of the Li metal. Similarly, other elements present in the Li metal surface are considered as the constituents from LiTFSI and LiNO$_3$ salts, as well as the electrolyte solvent, 1,3-dioxolane/1,2-dimethoxyethane (DOL/DME). The mass percentages of the elements are shown in ESI Table S1.†

To evaluate the chemical state of SEI formed on the Li metal surface during cell cycling, X-ray photoelectron spectroscopy (XPS) analysis was performed on the LMAs cycled in electrolyte with and without the Gd(NO$_3$)$_3$ additive. Fig. 2a shows the XPS spectra of the LMA surface cycled using the electrolyte without additive; it has no recognizable peaks for Gd compounds (Fig. 2b) as any Gd compound is absent. Conversely, the XPS spectra (Fig. 2d) of the LMA cycled using electrolyte with the additive shows the binding energy peaks of Gd-4d fitted at ~142.4 eV and ~138.8 eV, as shown in Fig. 2c, indicating Gd to be present in its +3-oxidation state in the SEI layer formed during LMA cycling.

ESI Table S2† shows the elemental ratios (%) of elements from XPS analyses for C 1s, N 1s, O 1s, F 1s, S 2p, and Li 1s while considering the sensitivity factors for each spectrum. It depicts that the SEI layers formed on the LMA using both batches of electrolyte consist of organic and inorganic compounds, such as (CH$_2$OCO$_2$Li)$_2$, (ROCO$_2$Li)$_2$, and LiF, as shown in ESI Fig. S2.† However, the SEI layer formed on the LMA, when it reacted with an electrolyte having Gd(NO$_3$)$_3$ additive, which contained lesser O, F, and S elements. This observation can be associated with LiTFSI salt in the electrolyte. This also suggests that the nitrate anions present in the electrolyte additive, Gd(NO$_3$)$_3$, restrain severe electrolyte decomposition and maintain Li inventory when the LiTFSI-based electrolyte reacts with the LMAs. In addition, the significantly higher ratio of Gd shown by SEM-EDS suggests that Gd is incorporated predominantly within the bulk of the LMA, rather than only in the surface modifications.

2.2. Electrochemical characterizations

To analyze and understand the effects of additive-engineered electrolytes in an electrochemical setting, electrochemical tests were performed on Li|Li symmetrical and full-cell configurations. To optimize the amount of additive required in the electrolyte, several symmetrical cells using electrolytes without Gd(NO$_3$)$_3$ and with Gd(NO$_3$)$_3$ additive in concentrations of 0.5, 1, 2, and 3 mg ml^{-1} were assembled and tested as described in ESI.† As shown in ESI Fig. S4a,† the electrolyte with 1 mg ml^{-1} of additive performed best among all the tests with longer

Fig. 2 XPS spectra for post-cycling LMA surfaces without (a and b) and with (c and d) $Gd(NO_3)_3$ electrolyte additive. Multiple scans are shown in (a).

plating/stripping hours of ~1000 h at lower overpotential voltages. This optimal additive amount of 1 mg ml^{-1} was calculated to be equivalent to 3 mM of $Gd(NO_3)_3$ additive in 1 M LiTFSI-$LiNO_3$ ether-based electrolyte.

Fig. 3 shows Nyquist plots from electrochemical impedance spectroscopy (EIS) analyses of Li symmetrical cells to analyze the charge transfer characteristics at fresh conditions and Li plating/stripping performance at different current densities, respectively. The use of $Gd(NO_3)_3$ additive in the electrolyte reduced the total charge transfer resistance from 130 Ω to 60 Ω as presented in Fig. 3a. This significant reduction in charge transfer resistance confirmed that the SEI layer was tuned well by the Gd additive, which resulted in the effective passivation of the LMA with a high ionically conductive passivation layer.

Similarly, Li symmetrical cells were cycled at constant current densities of 0.5 mA cm^{-2} (low) and 2 mA cm^{-2} (high) at 1 mA h cm^{-2} areal capacities. This was aimed to test their galvanostatic plating/stripping behavior. As shown in Fig. 3b, the cells with additives in the electrolyte performed stably for over 2000 hours, whereas the cells without additives became unstable, showing high overpotential only after 600 hours. Fig. 3c shows the voltage profiles of both types of cells in a mid-cycling period of 675 to 695 cycling hours. It can be observed that the symmetric cells cycled without the Gd additive in an electrolyte showed a significantly higher overpotential of approximately ± 70 mV, whereas those cycled with the additive-

containing electrolyte showed a suppressed overpotential value of about ±20 mV.

The lower overpotential during the plating/stripping of Li ions in the symmetrical cells cycled with additive indicates that the additive-tuned SEI layer reduces the energy barrier during the Li plating/stripping process, thus providing highly efficient passivation of the Li metal surface. Additionally, symmetrical cells with the additive cycled at a higher current density of 2 mA cm^{-2}, showed stable cycling for 1200 hours with an overpotential stabilized at approximately ±58 mV, whereas the cells without additive were stable for merely 200 hours with higher and even unstable overpotential, reaching up to ±300 mV (Fig. 3d).

2.3. Cell performances of additive-engineered electrolyte

To demonstrate the integration potential of practical Li metal batteries with high energy density, full cells with additive-engineered electrolytes were assembled and electrochemically tested. $LiFePO_4$ (LFP) cathode was initially employed as the active cathode material to construct Li- metal-based full cells. Detailed fabrication and cell assembly procedures are given in the Experimental section of the ESI.† The cycling stability, rate performance, and coulombic efficiency (CE) were evaluated with and without the Gd additive within the electrolyte.

The initial discharge capacities of LFP/Li cells during 0.2C formation cycles were 156.30 and 142.06 mA h g^{-1} with

Fig. 3 Electrochemical testing of Li symmetrical cells. (a) Nyquist plots obtained from the EIS test, galvanostatic plating/stripping cycle test, (b) current density of 0.5 mA cm^{-2} and capacity of 1 mA h cm^{-2}, (c) test profile between 675 to 695 cycling hours, and (d) current density 2 mA cm^{-2} and capacity of 1 mA h cm^{-2}.

coulombic efficiencies (CE) of 87.82% and 84.11%, respectively, when cycled with and without Gd(NO$_3$)$_3$ additive in the electrolyte. Additionally, as shown in ESI Fig. S5a,† the initial 1C discharge capacities post-formation cycles were 157.38 and 142.10 mA h g^{-1} with CE of 99.98% and 92.60%, respectively. The lower CE observed for the cells without the additive indicates that a greater number of Li ions were consumed at the interface during the SEI layer formation. With the inclusion of the Gd electrolyte additive, these side reactions are suppressed, leading to an increased CE value due to the preserved Li inventory during the formation of a highly stabilized SEI layer. The full cells were also tested at various C-rates (1C = 170 mA g^{-1} for LFP): 0.2, 0.5, 1, 2, and 5 and returned to 0.5C (Fig. 4a). The LFP/Li cells with the Gd electrolyte additive showed higher capacities than the cells without electrolyte additive at all tested C-rates (Table 1). When the C-rate returned to 0.5C, 98.33% of the initial capacity was retained in the cells with the Gd(NO$_3$)$_3$ additive. Simultaneously, the cells were tested at a constant rate of 1C to analyze their long-term cycling performance and capacity fading characteristics (Fig. 4b). The cells with electrolyte additives maintained a discharge capacity of 150.27 mA h g^{-1} at the 400th cycle, while those without the additive showed a discharge capacity of 92.96 mA h g^{-1} at the same cycle. These results further validate Gd(NO$_3$)$_3$ as a potential electrolyte additive to facilitate the formation of a stable SEI layer, nodular Li deposition morphology, Li dendrite inhibition, and suppression of side reactions.

As depicted in ESI Fig. S5b,† the initial discharge capacities of NMC/Li cells at 1C (1C = 200 mA g^{-1} for NMC111) were 92 and 119 mA h g^{-1} for the cells without additive and with

additive in the electrolytes; the initial CEs were 70.77% and 74.37%, respectively. This trend is consistent with that for the LFP/Li cells. The results of rate-capacity tests for the NMC/Li cells are illustrated in Fig. 4c, which do not exhibit significant differences between the electrolytes without and with the Gd(NO$_3$)$_3$ additive. However, capacity retention was slightly higher in the cells with Gd(NO$_3$)$_3$ than in the cells without additives at 89.91% *versus* 88.83%. The long-term capacity fading results are shown in Fig. 4d, where the cells with Gd(NO$_3$)$_3$ electrolyte show a more stable capacity retention after reaching a stabilized capacity of ∼110 mA h g^{-1}. They retained 96.82% of their stabilized capacity after 300 cycles, while the control cells without the Gd(NO$_3$)$_3$ electrolyte additive retained only 72.54% of their capacity after 300 cycles.

NMC/Li full cells were scanned at a scan rate of 0.5 mV s^{-1} from 0 to 5 V *versus* Li/Li$^+$ for linear sweep voltammetry (LSV) and from 2 to 4.5 V for cyclic voltammetry (CV) to investigate the effect of Gd(NO$_3$)$_3$ on high voltage stability of cells. The enlarged plots (ESI Fig. S4c,† inset) for cells cycled without electrolyte additive show multiple reduction peaks, indicating the prevalence of various side reactions and electrolyte reduction at the interface. In contrast, by including the optimal concentration of Gd(NO$_3$)$_3$ additive in the electrolyte, these parasitic reactions were suppressed as evidenced by a single reduction peak in the inset of ESI Fig. S4d.† Similarly, the LSV curve exhibited fluctuation beyond 4.3 V for cells without electrolyte additive, whereas a stable curve was observed for those with the Gd electrolyte additive (ESI Fig. S4c and d†). As the nitrate anion is already present in the base electrolyte without the additive, such stabilization could be attributed to the presence of Gd
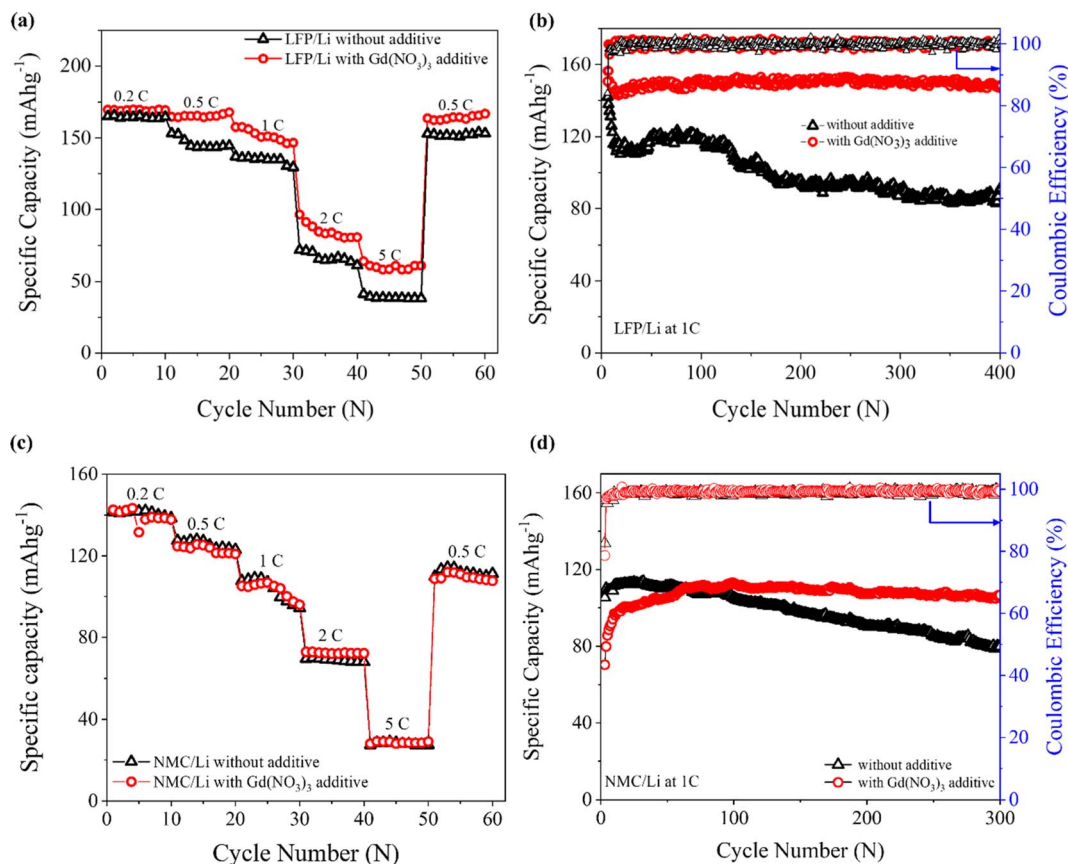
Fig. 4   LFP/Li (a and b) and NMC/Li (c and d) full cells cycled with and without the use of an additive in the electrolyte. (a and c) Rate capability and capacity retention tests; (b and d) long-term cycling tests at 1C.

Table 1   Specific capacities at various C-rates and LFP/Li cells. Values are also plotted in Fig. 4a

C-rate	Without additive	With Gd(III) nitrate additive
0.2C	165.08	169.83
0.5C	153.28	164.84
1C	137.05	157.69
2C	71.93	96.58
5C	41.23	64.15
0.5C recovery	150.84	166.99
Retention at 0.5C	91.37%	98.33%

compounds. Thus, the $Gd(NO_3)_3$ electrolyte additive promotes the high voltage stability of electrolytes under full-cell cycling conditions. As shown in ESI Fig. S4b,† oxidation-reduction peaks were observed in both cells containing electrolytes with and without additives. There was an increase in the oxidation peak potential from 3.9 V to 4.08 V for cells with the Gd additive as compared to cells without the additive. Similarly, the CV curves exhibited increased plating/stripping current values and a larger integrated CV curve area for cells cycled with the $Gd(NO_3)_3$ additive. This verifies the notion that the electrolyte additive enhances the kinetics of the electrochemical reaction in the cell and facilitates a lower energy barrier for Li-ion deposition, thus promoting cell cycling capacity and stability.

The charge transfer resistance (R_{ct}) of these full cells was measured at different cycle numbers as listed in ESI Table S3.† The full cells cycled in the presence of electrolyte additive showed very low R_{ct} compared to the cells without additive. This is again evidence that the $Gd(NO_3)_3$ electrolyte additive enhances the charge transfer and reaction kinetics within the full cell. Additionally, the decrease in R_{ct} for cells without the additive after 10 and 50 cycles can be credited to the Li dendrite formation on the LMA surface, resulting in increased electrolyte contact and consumption. Conversely, a similar response was observed for cells with $Gd(NO_3)_3$ additive, which is mainly attributed to the stabilization of the SEI layer after 10 and 50 cycles, promoting improved Li deposition in nodular morphology. This facilitates less contact area with the electrolyte and suppresses unwanted side reactions between the LMA and electrolyte.

3.   Conclusions

In summary, we have demonstrated that the incorporation of only 3 mM $Gd(NO_3)_3$ electrolyte additive in $LiTFSI$-$LiNO_3$ ether-based liquid electrolyte effectively tunes the composition of the SEI layer, suppresses the Li dendrite growth, and inhibits parasitic side chain reactions in the LMAs simultaneously. This electrolyte additive enables the nodular morphology of Li-ion

deposition in the Li metal surface and thus, promotes outstanding plating/stripping behavior in symmetrical cells. The nature of the additive is such that it initiates the sacrificial reaction with Li metal and passivates it at the interface by forming a stable SEI layer before electrolyte decomposition or Li-ion reduction can occur. The additive-engineered Li symmetrical cells show a nearly $4\times$ increment in plating/stripping hours, when cycled at a current density of 0.5 mA cm^{-2}, reaching a capacity of 1 mA h cm^{-2}. Similarly, the LFP/Li full cells cycled in an electrolyte with an additive exhibited exceptionally stable cycling performance and high CE compared to cells without the additive. The introduction of this novel additive in the electrolyte contributed to the formation of a stable SEI layer and conformal passivation of the Li metal. This work successfully mitigates the prime hurdle of SEI instability and Li dendrite growth in the LMAs and provides insights into electrolytes engineered with nitrate ion additive for the development of high-energy density LMBs.

Data availability

The data that support the findings of this study are available from the corresponding author upon reasonable request. Due to privacy restrictions, the data are not publicly available. Data includes experimental findings and detailed characterizations. Additional information and materials are available from the corresponding author upon reasonable request.

Conflicts of interest

The authors declare no competing interests.

Acknowledgements

References

1 W. Xu, J. Wang, F. Ding, X. Chen, E. Nasybulin, Y. Zhang and J.-G. Zhang, *Energy Environ. Sci.*, 2014, **7**, 513–537.

2 J. Liu, T. Qian, N. Xu, M. F. Wang, J. Q. Zhou, X. W. Shen and C. L. Yan, *Energy Storage Mater.*, 2020, **24**, 265–271.

3 X. J. Liu, T. Qian, M. F. Wang, H. L. Chen and C. L. Yan, *Energy Storage Mater.*, 2019, **17**, 260–265.

4 A. Gurung and Q. Qiao, *Joule*, 2018, **2**, 1217–1230.

5 A. Gurung, K. Chen, R. Khan, S. S. Abdulkarim, G. Varnekar, R. Pathak, R. Naderi and Q. Qiao, *Adv. Energy Mater.*, 2017, 1602105.

6 A. Gurung, K. M. Reza, S. Mabrouk, B. Bahrami, R. Pathak, B. S. Lamsal, S. I. Rahman, N. Ghimire, R. S. Bobba and K. Chen, *Adv. Funct. Mater.*, 2020, **30**, 2001865.

7 P. Albertus, S. Babinec, S. Litzelman and A. Newman, *Nat. Energy*, 2018, **3**, 16–21.

8 S. S. Zhang, *J. Power Sources*, 2006, **162**, 1379–1394.

9 M. Balasubramanian, H. S. Lee, X. Sun, X.-Q. Yang, A. Moodenbaugh, J. McBreen, D. A. Fischer and Z. Fu, *Electrochem. Solid-State Lett.*, 2001, **5**, A22.

10 L. Lu, X. Han, J. Li, J. Hua and M. Ouyang, *J. Power Sources*, 2013, **226**, 272–288.

11 J. Vetter, P. Novák, M. R. Wagner, C. Veit, K.-C. Möller, J. Besenhard, M. Winter, M. Wohlfahrt-Mehrens, C. Vogler and A. Hammouche, *J. Power Sources*, 2005, **147**, 269–281.

12 P. Verma, P. Maire and P. Novák, *Electrochim. Acta*, 2010, **55**, 6332–6341.

13 V. Etacheri, R. Marom, R. Elazari, G. Salitra and D. Aurbach, *Energy Environ. Sci.*, 2011, **4**, 3243–3262.

14 K. J. Harry, D. T. Hallinan, D. Y. Parkinson, A. A. MacDowell and N. P. Balsara, *Nat. Mater.*, 2014, **13**, 69–73.

15 R. Khurana, J. L. Schaefer, L. A. Archer and G. W. Coates, *J. Am. Chem. Soc.*, 2014, **136**, 7395–7402.

16 D. Zhou, R. Liu, Y. B. He, F. Li, M. Liu, B. Li, Q. H. Yang, Q. Cai and F. Kang, *Adv. Energy Mater.*, 2016, **6**, 1502214.

17 A. Baniya, A. Gurung, J. Pokharel, K. Chen, R. Pathak, B. S. Lamsal, N. Ghimire, R. S. Bobba, S. I. Rahman and S. Mabrouk, *ACS Appl. Energy Mater.*, 2022, **5**(1), 648–657.

18 A. Basile, A. Bhatt and A. O'Mullane, *Nat. Commun.*, 2016, **7**, 1–11.

19 A. I. Bhatt, A. S. Best, J. Huang and A. F. Hollenkamp, *J. Electrochem. Soc.*, 2009, **157**, A66.

20 A. Basile, A. F. Hollenkamp, A. I. Bhatt and A. P. O'Mullane, *Electrochem. Commun.*, 2013, **27**, 69–72.

21 H. L. Chen, J. Liu, X. Zhou, H. Q. Ji, S. S. Liu, M. F. Wang, T. Qian and C. L. Yan, *Chem. Eng. J.*, 2021, **404**, 8.

22 F. Ding, W. Xu, G. L. Graff, J. Zhang, M. L. Sushko, X. Chen, Y. Shao, M. H. Engelhard, Z. Nie and J. Xiao, *J. Am. Chem. Soc.*, 2013, **135**, 4450–4456.

23 J. Qian, W. A. Henderson, W. Xu, P. Bhattacharya, M. Engelhard, O. Borodin and J.-G. Zhang, *Nat. Commun.*, 2015, **6**, 1–9.

24 N. W. Li, Y. X. Yin, C. P. Yang and Y. G. Guo, *Adv. Mater.*, 2016, **28**, 1853–1858.

25 E. Kazyak, K. N. Wood and N. P. Dasgupta, *Chem. Mater.*, 2015, **27**, 6457–6462.

26 R. Pathak, K. Chen, A. Gurung, K. M. Reza, B. Bahrami, F. Wu, A. Chaudhary, N. Ghimire, B. Zhou and W. H. Zhang, *Adv. Energy Mater.*, 2019, **9**, 1901486.

27 R. Pathak, K. Chen, A. Gurung, K. M. Reza, B. Bahrami, J. Pokharel, A. Baniya, W. He, F. Wu and Y. Zhou, *Nat. Commun.*, 2020, **11**, 1–10.

28 K. Chen, R. Pathak, A. Gurung, E. A. Adhamash, B. Bahrami, Q. He, H. Qiao, A. L. Smirnova, J. J. Wu and Q. Qiao, *Energy Storage Mater.*, 2019, **18**, 389–396.

29 J. M. Kim, M. H. Engelhard, B. Y. Lu, Y. B. Xu, S. Tan, B. E. Matthews, S. Tripathi, X. Cao, C. J. Niu, E. Y. Hu, S. M. Bak, C. M. Wang, Y. S. Meng, J. G. Zhang and W. Xu, *Adv. Funct. Mater.*, 2022, **32**, 9.

30 S. Choudhury, Z. J. Huang, C. V. Amanchukwu, P. E. Rudnicki, Y. L. Chen, D. T. Boyle, J. Qin, Y. Cui and Z. A. Bao, *Adv. Energy Mater.*, 2023, **13**, 11.

31 K. Chen, R. Pathak, A. Gurung, K. M. Reza, N. Ghimire, J. Pokharel, A. Baniya, W. He, J. J. Wu and Q. Q. Qiao, *J. Mater. Chem. A*, 2020, **8**, 1911–1919.

32 G. Zheng, S. W. Lee, Z. Liang, H.-W. Lee, K. Yan, H. Yao, H. Wang, W. Li, S. Chu and Y. Cui, *Nat. Nanotechnol.*, 2014, **9**, 618–623.

33 D. Lin, Y. Liu, Z. Liang, H.-W. Lee, J. Sun, H. Wang, K. Yan, J. Xie and Y. Cui, *Nat. Nanotechnol.*, 2016, **11**, 626–632.

34 K. Yan, Z. Lu, H.-W. Lee, F. Xiong, P.-C. Hsu, Y. Li, J. Zhao, S. Chu and Y. Cui, *Nat. Energy*, 2016, **1**, 1–8.

35 S. T. Oyakhire, W. B. Zhang, A. Shin, R. Xu, D. T. Boyle, Z. A. Yu, Y. S. Ye, Y. F. Yang, J. A. Raiford, W. Huang, J. R. Schneider, Y. Cui and S. F. Bent, *Nat. Commun.*, 2022, **13**, 12.

36 Y. Gu, E. M. You, J. D. Lin, J. H. Wang, S. H. Luo, R. Y. Zhou, C. J. Zhang, J. L. Yao, H. Y. Li, G. Li, W. W. Wang, Y. Qiao, J. W. Yan, D. Y. Wu, G. K. Liu, L. Zhang, J. F. Li, R. Xu, Z. Q. Tian and B. W. Mao, *Nat. Commun.*, 2023, **14**, 11.

37 D. Lin, Y. Liu and Y. Cui, *Nat. Nanotechnol.*, 2017, **12**, 194–206.

38 X.-B. Cheng, R. Zhang, C.-Z. Zhao and Q. Zhang, *Chem. Rev.*, 2017, **117**, 10403–10473.

39 S. Li, M. Jiang, Y. Xie, H. Xu, J. Jia and J. Li, *Adv. Mater.*, 2018, **30**, 1706375.

40 H. Yang, C. Guo, A. Naveed, J. Lei, J. Yang, Y. Nuli and J. Wang, *Energy Storage Mater.*, 2018, **14**, 199–221.

41 J. Lang, L. Qi, Y. Luo and H. Wu, *Energy Storage Mater.*, 2017, **7**, 115–129.

42 Y. Ma, Z. Zhou, C. Li, L. Wang, Y. Wang, X. Cheng, P. Zuo, C. Du, H. Huo and Y. Gao, *Energy Storage Mater.*, 2018, **11**, 197–204.

43 W. Wahyudi, V. Ladelta, L. Tsetseris, M. M. Alsabban, X. Guo, E. Yengel, H. Faber, B. Adilbekova, A. Seitkhan and A. H. Emwas, *Adv. Funct. Mater.*, 2021, 2101593.

44 Y. Qian, S. Hu, X. Zou, Z. Deng, Y. Xu, Z. Cao, Y. Kang, Y. Deng, Q. Shi and K. Xu, *Energy Storage Mater.*, 2019, **20**, 208–215.

45 J. Fu, X. Ji, J. Chen, L. Chen, X. Fan, D. Mu and C. Wang, *Angew. Chem.*, 2020, **132**, 22378–22385.

46 J. Zheng, M. H. Engelhard, D. Mei, S. Jiao, B. J. Polzin, J.-G. Zhang and W. Xu, *Nat. Energy*, 2017, **2**, 1–8.

47 Y. Yamada, J. Wang, S. Ko, E. Watanabe and A. Yamada, *Nat. Energy*, 2019, **4**, 269–280.

48 B. D. Adams, E. V. Carino, J. G. Connell, K. S. Han, R. Cao, J. Chen, J. Zheng, Q. Li, K. T. Mueller and W. A. Henderson, *Nano Energy*, 2017, **40**, 607–617.

49 T. T. Beyene, H. K. Bezabh, M. A. Weret, T. M. Hagos, C.-J. Huang, C.-H. Wang, W.-N. Su, H. Dai and B.-J. Hwang, *J. Electrochem. Soc.*, 2019, **166**, A1501.

50 R. Weber, M. Genovese, A. Louli, S. Hames, C. Martin, I. G. Hill and J. Dahn, *Nat. Energy*, 2019, **4**, 683–689.

51 W. Xue, Z. Shi, M. Huang, S. Feng, C. Wang, F. Wang, J. Lopez, B. Qiao, G. Xu and W. Zhang, *Energy Environ. Sci.*, 2020, **13**, 212–220.

52 S. Lin and J. Zhao, *ACS Appl. Mater. Interfaces*, 2020, **12**, 8316–8323.

53 Z. Xie, X. An, Z. Wu, X. Yue, J. Wang, X. Hao, A. Abudula and G. Guan, *J. Mater. Sci. Technol.*, 2021, **74**, 119–127.

54 Y. Yamada, K. Usui, K. Sodeyama, S. Ko, Y. Tateyama and A. Yamada, *Nat. Energy*, 2016, **1**, 1–9.

55 R. Younesi, M. Hahlin, M. Roberts and K. Edström, *J. Power Sources*, 2013, **225**, 40–45.

56 J. Zheng, M. Gu, H. Chen, P. Meduri, M. H. Engelhard, J.-G. Zhang, J. Liu and J. Xiao, *J. Mater. Chem. A*, 2013, **1**, 8464–8470.

57 J. Zheng, H. Zheng, R. Wang, L. Ben, W. Lu, L. Chen, L. Chen and H. Li, *Phys. Chem. Chem. Phys.*, 2014, **16**, 13229–13238.

58 K. Edstroem, T. Gustafsson and J. O. Thomas, *Electrochim. Acta*, 2004, **50**, 397–403.

59 H. Li, D. Chao, B. Chen, X. Chen, C. Chuah, Y. Tang, Y. Jiao, M. Jaroniec and S.-Z. Qiao, *J. Am. Chem. Soc.*, 2020, **142**, 2012–2022.

60 Z. Yu, Y. Cui and Z. Bao, *Cell Rep. Phys. Sci.*, 2020, **1**, 100119.

61 W. Li, H. Yao, K. Yan, G. Zheng, Z. Liang, Y.-M. Chiang and Y. Cui, *Nat. Commun.*, 2015, **6**, 1–8.

62 A. Rosenman, R. Elazari, G. Salitra, E. Markevich, D. Aurbach and A. Garsuch, *J. Electrochem. Soc.*, 2015, **162**, A470.

63 S. Liu, G.-R. Li and X.-P. Gao, *ACS Appl. Mater. Interfaces*, 2016, **8**, 7783–7789.

64 R. Cao, W. Xu, D. Lv, J. Xiao and J. G. Zhang, *Adv. Energy Mater.*, 2015, **5**, 1402273.

65 W. Jia, C. Fan, L. Wang, Q. Wang, M. Zhao, A. Zhou and J. Li, *ACS Appl. Mater. Interfaces*, 2016, **8**, 15399–15405.

66 Z. Lin, Z. Liu, W. Fu, N. J. Dudney and C. Liang, *Adv. Funct. Mater.*, 2013, **23**, 1064–1069.

67 F. Wu, J. T. Lee, N. Nitta, H. Kim, O. Borodin and G. Yushin, *Adv. Mater.*, 2015, **27**, 101–108.

68 Y. Liu, D. Lin, Y. Li, G. Chen, A. Pei, O. Nix, Y. Li and Y. Cui, *Nat. Commun.*, 2018, **9**, 1–10.

69 X.-Q. Zhang, X. Chen, L.-P. Hou, B.-Q. Li, X.-B. Cheng, J.-Q. Huang and Q. Zhang, *ACS Energy Lett.*, 2019, **4**, 411–416.

70 J.-J. Woo, V. A. Maroni, G. Liu, J. T. Vaughey, D. J. Gosztola, K. Amine and Z. Zhang, *J. Electrochem. Soc.*, 2014, **161**, A827.

71 T. Doi, Y. Shimizu, M. Hashinokuchi and M. Inaba, *J. Electrochem. Soc.*, 2017, **164**, A6412.

72 Z. Zeng, V. Murugesan, K. S. Han, X. Jiang, Y. Cao, L. Xiao, X. Ai, H. Yang, J.-G. Zhang and M. L. Sushko, *Nat. Energy*, 2018, **3**, 674–681.

73 C. Yan, Y. X. Yao, X. Chen, X. B. Cheng, X. Q. Zhang, J. Q. Huang and Q. Zhang, *Angew. Chem.*, 2018, **130**, 14251–14255.

74 C. Yan, X. B. Cheng, Y. Tian, X. Chen, X. Q. Zhang, W. J. Li, J. Q. Huang and Q. Zhang, *Adv. Mater.*, 2018, **30**, 1707629.

75 N. D. Trinh, D. Lepage, D. Aymé-Perrot, A. Badia, M. Dollé and D. Rochefort, *Angew. Chem., Int. Ed.*, 2018, **57**, 5072–5075.

76 Y. Sun, Y. Zhao, J. Wang, J. Liang, C. Wang, Q. Sun, X. Lin, K. R. Adair, J. Luo and D. Wang, *Adv. Mater.*, 2019, **31**, 1806541.

77 K. Pranay Reddy, P. Fischer, M. Marinaro and M. Wohlfahrt-Mehrens, *ChemElectroChem*, 2018, **5**, 2758–2766.

78 X. Xu, J. Liu, Z. Liu, J. Shen, R. Hu, J. Liu, L. Ouyang, L. Zhang and M. Zhu, *ACS Nano*, 2017, **11**, 9033–9040.

79 K. N. Wood, M. Noked and N. P. Dasgupta, *ACS Energy Lett.*, 2017, **2**, 664–672.

80 Y. Liu, D. Lin, P. Y. Yuen, K. Liu, J. Xie, R. H. Dauskardt and Y. Cui, *Adv. Mater.*, 2017, **29**, 1605531.

81 C. Fang, X. Wang and Y. S. Meng, *Trends Chem.*, 2019, **1**, 152–158.

82 S. Jiao, X. Ren, R. Cao, M. H. Engelhard, Y. Liu, D. Hu, D. Mei, J. Zheng, W. Zhao and Q. Li, *Nat. Energy*, 2018, **3**, 739–746.

83 J. Alvarado, M. A. Schroeder, T. P. Pollard, X. Wang, J. Z. Lee, M. Zhang, T. Wynn, M. Ding, O. Borodin and Y. S. Meng, *Energy Environ. Sci.*, 2019, **12**, 780–794.

84 J. Zheng, G. Ji, X. Fan, J. Chen, Q. Li, H. Wang, Y. Yang, K. C. DeMella, S. R. Raghavan and C. Wang, *Adv. Energy Mater.*, 2019, **9**, 1803774.

85 L. Li, S. Basu, Y. Wang, Z. Chen, P. Hundekar, B. Wang, J. Shi, Y. Shi, S. Narayanan and N. Koratkar, *Science*, 2018, **359**, 1513–1516.

86 H. S. Wang, Z. Yu, X. Kong, S. C. Kim, D. T. Boyle, J. Qin, Z. N. Bao and Y. Cui, *Joule*, 2022, **6**, 588–616.

87 X. Ren, S. Chen, H. Lee, D. Mei, M. H. Engelhard, S. D. Burton, W. Zhao, J. Zheng, Q. Li and M. S. Ding, *Chem*, 2018, **4**, 1877–1892.

88 S. Chen, J. Zheng, D. Mei, K. S. Han, M. H. Engelhard, W. Zhao, W. Xu, J. Liu and J. G. Zhang, *Adv. Mater.*, 2018, **30**, 1706102.

89 Y. Yamada and A. Yamada, *J. Electrochem. Soc.*, 2015, **162**, A2406.

90 J. Zheng, P. Yan, D. Mei, M. H. Engelhard, S. S. Cartmell, B. J. Polzin, C. Wang, J. G. Zhang and W. Xu, *Adv. Energy Mater.*, 2016, **6**, 1502151.

91 X. Fan, L. Chen, O. Borodin, X. Ji, J. Chen, S. Hou, T. Deng, J. Zheng, C. Yang and S.-C. Liou, *Nat. Nanotechnol.*, 2018, **13**, 715–722.